RSC Advances

PAPER

View Article Online
View Journal | View Issue

Cite this: *RSC Adv.*, 2021, **11**, 31795

Electrospun cationic nanofiber membranes for adsorption and determination of Cr(VI) in aqueous solution: adsorption characteristics and discoloration mechanisms

Run Fang, *[ab] Bing-Chiuan Shiu,[ab] Yuansong Ye,[ab] Yuchi Zhang,[ab] Hanyu Xue,[ab] Ching-Wen Lou[acdfg] and Jia-Horng Lin *[acdef]

In this study, a novel cationic nanofiber membrane with various functional groups, good structural stability, and high adsorption capacity of Cr(VI) is presented. This nanofiber membrane is prepared by electrospinning a mixed aqueous solution of a cationic polycondensate (CP) and polyvinyl alcohol (PVA). With the aid of PVA, CP can be smoothly electrospun without using any organic solvents, and the cross-linking between CP and PVA improves the stability of membrane in acidic solution. Chemical and morphology characterization reveals that the CP/PVA membrane is composed of interwoven nanofibers that contain numerous cationic groups. Due to its high cationicity and hydrophilicity, the CP/PVA membrane shows great affinity for $HCr_2O_7^-$ and $Cr_2O_7^{2-}$. Adsorption experiments indicate that the CP/PVA membrane can remove Cr(VI) from simulated wastewater rapidly and efficiently in both batch and continuous mode. Besides, the presence of most coexisting ions will not interfere with the adsorption. Due to the redox reaction between the CP/PVA membrane and adsorbed Cr(VI), the CP/PVA membrane exhibits distinct color change after Cr(VI) adsorption and the discoloration is highly dependent on the adsorption amount. Therefore, in addition to serving as a highly efficient adsorbent, the CP/PVA membrane is also expected to be a convenient and low-cost method for semi-quantitative determination of Cr(VI) in wastewater.

Received 4th August 2021
Accepted 1st September 2021

DOI: 10.1039/d1ra05917c

rsc.li/rsc-advances

1. Introduction

Plating, textile dyeing, and metal processing industries generate a considerable amount of chromium-containing wastewaters. Cr(VI) in the wastewaters is highly mobile and carcinogenic, which can be collected and transported along the food chain and cause permanent damage to the human body and plants.[1] The large-scale Cr(VI) treatment usually consists of two steps: reduction and precipitation. Cr(VI) is first reduced to Cr(III) under acidic conditions by a reducing agent. Then, the pH of the wastewater is increased and the Cr(III) is turned into $Cr(OH)_3$, which is thereafter removed by coagulation and precipitation.[2] Nonetheless, this method inevitably creates a large quantity of mixed sludge containing multiple hydroxides, and brings troublesome secondary pollutions. To overcome the dilemma, many convenient and efficient processing techniques have been developed, such as electrochemical treatment, photocatalytic reduction, ion exchange, and adsorption.[3–5] In particular, adsorption method has the advantages of low energy cost, easy operation process, and mild operation conditions, which can be either concurrently used with reduction-precipitation method or membrane separation, or used alone to deal with chromium-containing wastewater consisting of simple components. Therefore, numerous novel adsorbents for Cr(VI) removal, including modified biomass, graphene oxide, MOFs and nanoparticles, have been reported in recent years.[6–10] Although some of them have extremely high adsorption capacity, the complex preparation process and high cost of raw materials restrict their large-scale application to a certain extent.

Chromium-containing wastewater is usually acidic. Unlike most heavy metal ions, Cr(VI) is mainly present in $HCr_2O_7^-$ and $Cr_2O_7^{2-}$ anion state in an acidic aqueous solution, and the adsorbents with cationic functional groups usually have high

[a]*Department of Material and Chemical Engineering, Minjiang University, Fuzhou 350108, China. E-mail: jhlin@fcu.edu.tw; readfung@163.com; Tel: +886 4 24518661; +86 591 83761630*

[b]*Fujian Engineering and Research Center of New Chinese Lacquer Materials, Fuzhou 350108, China*

[c]*Innovation Platform of Intelligent and Energy-Saving Textiles, School of Textile Science and Engineering, Tiangong University, Tianjin 300387, China*

[d]*Advanced Medical Care and Protection Technology Research Center, College of Textile and Clothing, Qingdao University, Shandong 266071, China*

[e]*Laboratory of Fiber Application and Manufacturing, Department of Fiber and Composite Materials, Feng Chia University, Taichung 40724, Taiwan, China*

[f]*School of Chinese Medicine, China Medical University, Taichung 40402, Taiwan, China*

[g]*Department of Bioinformatics and Medical Engineering, Asia University, Taichung 41354, Taiwan, China*

affinity for Cr(VI).[11] Therefore, it is a simple and effective strategy to improve the adsorption capacity of Cr(VI) by designing the molecular structure of adsorbents based on electrostatic interaction. In addition to the design of chemical structure, the optimization of adsorbent morphology is another effective measure to improve the adsorption efficiency. Comparing to many lumpy, granular, or spherical adsorbents, nanofiber membranes made by electrospinning have larger specific surface areas and considerably high porosity. Moreover, a large diversity of functional groups can be immobilized onto nanofibers by means of grafting reaction.[12] These characteristics significantly improve the adsorption capacity, water flux, and mass transfer rate of nanofiber membranes, facilitating the metal ion adsorption effectively.[13,14] As a result, nanofiber membranes with cationic groups have become a research hotspot in the field of Cr(VI)-containing wastewater treatment.

Two main methods are commonly used for producing nanofiber membranes with adsorption capacity of Cr(VI). The first one is to prepare cationic nanofiber membranes directly by electrospinning polymers containing cationic groups. Chitosan and some cellulose derivatives are the most representative polymers for this method because they contain amine groups that can be protonated in acidic solution.[15–18] However, the relatively low content of amine groups contained by these nanofiber membranes leads to fewer adsorption sites. So in many cases, chitosan and cellulose derivatives need to be further modified to achieve higher adsorption capacity of Cr(VI). Moreover, the poor stability of chitosan in strong acidic solution is also a problem affecting its practical application. The second method consists of two steps: the electrospinning of nanofibers and the modification of membranes. Polymers that have reactive groups like hydroxymethyl and cyano groups were electrospun to yield uncharged nanofiber membranes. Then, the membranes undergo surface modification and the functional groups that demonstrate strong affinity to metal ions, such as amine, thiol and carboxyl groups were immobilized on the fiber surface.[19–23] Although abundant functional groups, including cationic groups, can be grafted on the surface of nanofibers by this method, complex operations, highly active monomers and precise condition control are needed to obtain the ideal modification effect.

In this study, we present a novel cationic nanofiber membrane with various functional groups, good stability in acidic solution, and high adsorption capacity of Cr(VI). This nanofiber membrane is prepared by directly electrospinning a mixed aqueous solution of a cationic polycondensate (CP) and polyvinyl alcohol (PVA). Different from most cationic polymers that are prepared by free radical polymerization/copolymerization or natural polymer modification, the proposed CP is synthesized by polycondensation using inexpensive and readily available monomers and could be readily grafted and cross-linked because of its abundant functional groups. With the aid of PVA, nanofiber membranes can be conveniently electrospun without using any organic solvents. In order to evaluate the potential application of CP/PVA membranes in the removal of Cr(VI) from wastewater, batch and continuous adsorption experiments were performed and the effect of solution pH, adsorption time, initial Cr(VI) concentration, and coexisting ions on the adsorption capacity were systematically studied. Finally, the discoloration phenomenon of CP/PVA membranes caused by Cr(VI) adsorption was also investigated.

2. Experimental

2.1 Materials

Triethylenetetramine, acetone, formaldehyde (37 wt% in aqueous solution), glutaraldehyde (GA, 50 wt% in aqueous solution), potassium polyvinyl sulfate (PVSK), diphenylcarbazide (DPC), polyvinyl alcohol (PVA-1799), Triton X-100, $K_2Cr_2O_7$, $CuCl_2 \cdot 2H_2O$, $NiCl_2 \cdot 6H_2O$, $ZnCl_2$, Na_2SO_4, $NaNO_3$, and NaCl were of analytical or biochemical reagent grade and purchased from Aladdin Industrial Co., Ltd. The number average molecular weight (M_n) of PVA-1799 was about 75 000 and the alcoholysis degree was 99%.

2.2 Preparation of CP/PVA nanofiber membranes

CP was synthesized using the aqueous polycondensation method described in our previous study.[24] Firstly, triethylenetetramine (30 mL), formaldehyde (40 mL), and acetone (36 mL) were added to a three-necked flask equipped with a condensate reflux and a mechanical stirrer. Hydrochloric acid was then used to adjust pH = 3, and the mixtures were blended at room temperature for one hour to have intermediate products. Next, the second batch of formaldehyde (36 mL) was added and the mixtures were adjusted to pH = 8 with a sodium hydroxide solution. The mixtures were heated to 60 °C and kept for reaction for 40 min, thereby obtaining orange CP aqueous solutions. CP aqueous solutions were thereafter infused to a semi-permeable tubing, and the salt and oligomer in the solution were removed by dialysis in deionized water. Finally, the purified solutions were condensed to form CP solutions with a solid content 15 wt% and then used to formulate the electrospinning solutions.

The CP solutions (20 mL) were infused into a conical flask that is placed in a water bath and heated to 85 °C, after which different amounts of PVA powders and 0.1 mL Triton X-100 were added and magnetically stirred until PVA is completely dissolved in the solutions. The solutions were left stand for 3 h and then electrospinning was conducted to produce nanofiber membranes with electrospinning voltage being 15.3 kV, a jet rate being 0.5 mL h^{-1}, a collection distance being 10 cm, a humidity being 35 ± 5%, and a collection media being PET nonwoven fabrics. Afterwards, the nanofiber membranes were vacuum dried at 60 °C for 6 h and then placed in a desiccator, the bottom of which was added with 10 mL of GA. The GA vapor reacted with the amine and hydroxyl groups on CP and PVA for 12 h, expediting the inter-crosslinking between them.[25,26] Finally, the nanofiber membranes were dried again and the crosslinked samples were used for subsequent experiments. Fig. 1 shows the preparation steps of CP/PVA membranes.

2.3 Characterization of CP/PVA membranes

Purified CP powders were dissolved in deionized water and the PVSK colloidal titration was employed to measure the

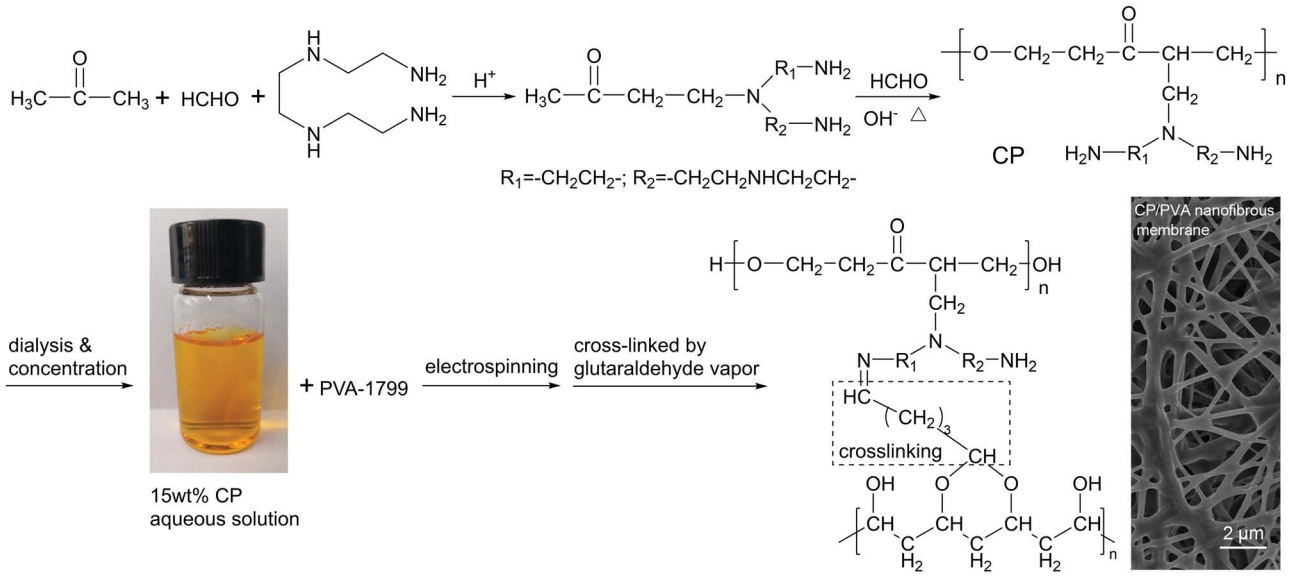

Fig. 1 Preparation of CP/PVA nanofiber membranes.

cationicity as related to pH values.[27] GPC (P230, Dalian Elite, China) was used to measure the molecular weight and molecular weight distribution of CP with Agilent PL aquagel-OH column. Modular Rheometer System (Mars60, Thermo Scientific, U.S.) was used to measure the viscosity of CP/PVA electrospining solutions as related to the CP/PVA ratio. The functional groups of cross-linked CP/PVA membranes as well as control samples were analyzed using FT-IR spectrometer (iS50, Thermo Nicolet, U.S.) in the region of 500–4000 cm^{-1} and the surface morphology was observed using SEM (SU8010, Hitachi, Japan). The CP/PVA membranes were cut into 10 × 100 mm long strips, and the tensile strength was measured at the speed of 10 mm min^{-1} using a universal testing machine (HT2402, Hungta, China).

2.4 Batch adsorption and regeneration experiments

The dried $K_2Cr_2O_7$ (0.2828 g) was weighed and dissolved in deionized water, formulating a stock solution with a specified volume being 1 L and a concentration being 100 mg L^{-1}, which was used in the static adsorption experiments. To evaluate the removal ability of CP/PVA membranes toward real Cr(VI) wastewater, a Cr(VI) containing wastewater sample provided by an electroplating enterprise was also used in the experiments.

During the adsorption experiments, 50 mL of $K_2Cr_2O_7$ solution (50 mg L^{-1}) or real wastewater was infused into a 250 mL flask, after which different mass of CP/PVA membranes were cut into 5 × 5 mm small pieces and added into the flask. Next, 0.5 mol L^{-1} HCl and NaOH solutions were used to adjust the pH value as desired and the flask was thereafter placed in a water bath shaker that operated at a rate of 150 rpm. The adsorption was performed for a certain length of time, and then the solution was filtered to have the post-adsorption solutions. With diphenylcarbazide being the chromogenic agent, a UV-Vis spectrophotometer (UV-2450, Shimadzu, Japan) was used to record the absorbance of the complex at 540 nm and the Cr(VI) concentration was calculated according to the standard curve.[28]. The equilibrium adsorption capacity q_e (mg Cr(VI)/g dry membrane) was computed with the equation as follows:

$$q_e = \frac{(C_0 - C_e)V}{m} \quad (1)$$

where C_0 and C_e is individually the initial concentration and equilibrium adsorption concentration (mg L^{-1}); V is the solution volume (L); and m is the dosage of adsorbent (g). The data was collected from three experiment results and averaged. When studying the influence of coexisting ions, an appropriate amount of $CuCl_2 \cdot 2H_2O$, $NiCl_2 \cdot 6H_2O$, $ZnCl_2$, Na_2SO_4, $NaNO_3$, and NaCl was separately dissolved in deionized water, after which $K_2Cr_2O_7$ was added into the different ion solutions. In each ion solution, Cr(VI) and the interfering ion (Cu^{2+}, Ni^{2+}, Zn^{2+}, SO_4^{2-}, NO_3^-, or Cl^-) separately had a concentration of 50 mg L^{-1}. The preferential adsorption of Cr(VI) among metal ions was investigated using a mixed-ion solution containing identical concentration of Cr(VI), Cu^{2+}, Ni^{2+} and Zn^{2+}. ICP-OES (720, Agilent, USA) was used to measure the original and residual concentrations of the four ions in the solution before and after adsorption. In the regeneration of adsorbents, the Cr(VI)-loaded CP/PVA membranes were added to a flask, NaOH solution (0.5 mol L^{-1}) and HCl solution (0.5 mol L^{-1}) were then added and shaked to elute the adsorbed Cr(VI) successively. After that, deionized water was used to wash the membranes until neutral. The adsorption capacity of regenerated CP/PVA membranes were tested following the aforementioned batch adsorption method.

2.5 Continuous adsorption and discoloration phenomenon

Continuous adsorption experiments were performed using a series of detachable filters, which are connected to form an adsorption column (Fig. 2). CP/PVA membranes were trimmed

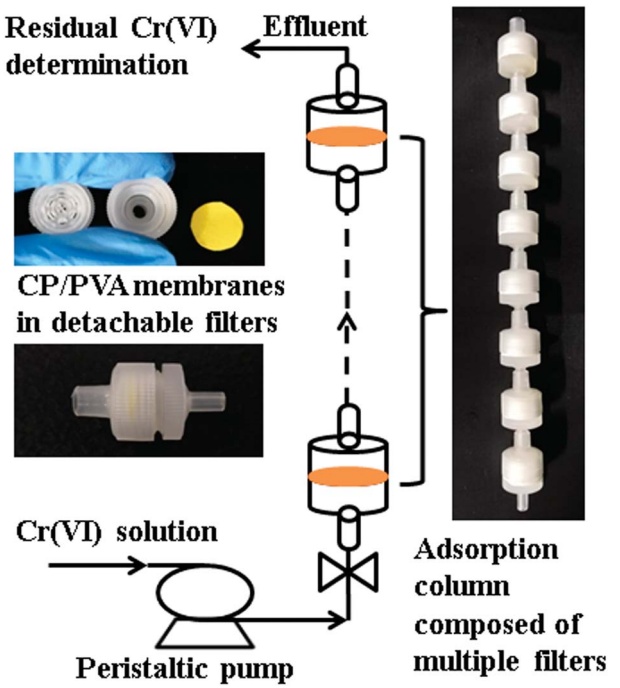

Fig. 2 Schematic diagram of continuous adsorption device.

along with the substrate into circular specimens with a diameter of 14 mm and a mass of 8 mg, and packed in the filters. 10 mg L^{-1} of Cr(VI) solution was pumped upward through the filter column at a flow rate of 4 mL min^{-1} using a peristaltic pump. The concentration of residual Cr(VI) in the effluent was determined regularly and the breakthrough curves were thereafter plotted. The amount of adsorbed Cr(VI) per gram of dry membrane at bed exhaustion, q_{exh} (mg g^{-1}) was calculated according to the following equation:

$$q_{total}(\text{mg}) = \frac{vA}{1000} = \frac{v}{1000}\int_0^t (C_0 - C_t)\mathrm{d}t \quad (2)$$

$$q_{exh}\left(\text{mg g}^{-1}\right) = \frac{q_{total}}{m} \quad (3)$$

where v is the flow rate (mL min^{-1}), m is the mass of the membrane (g), C_0 is the initial Cr(VI) concentration (mg L^{-1}), C_t is the residual Cr(VI) concentration in the effluent (mg L^{-1}). After continuous adsorption, the color changes of CP/PVA membranes related to the variation of adsorption amount of Cr(VI) were studied. The chemical state analysis of Cr and C elements and the discoloration mechanism of CP/PVA membranes were investigated using XPS analyzer (K-alpha Thermo Scientific, U.S).

3. Results and discussion

3.1 Chemical and morphology characterizations

GPC analysis indicated that CP had a number-average molecular weight (M_n) being 10 300, a weight-average molecular weight (M_w) being 18 100, and a polydispersity coefficient (M_w/M_n) being 1.76. Although CP has a lower molecular weight, the molecular structure shown in Fig. 1 indicates that it contains many polar groups, including amine, hydroxyl, carbonyl, and ether bond. Fig. 3a compares the FT-IR spectra of CP/PVA membranes as related to the CP/PVA ratio. The adsorption peaks at 1090 and 1050 cm^{-1} are attributed to C–O stretching vibration of hydroxyl and C–N stretching vibration of amine, respectively. The relative intensity of C–O peak decreases with increasing CP content, while that of C–N peak increases simultaneously. Meanwhile, the adsorption peak at 3200–3400 cm^{-1} shifts toward high wavenumbers. These characteristic peaks indicate that CP/PVA membranes contain a large quantity of –OH and $-NH_2$ and the peak intensity variation indicates that a rise in the CP ratio has a positive influence on the $-NH_2$ content of the membranes.[29] Comparing to pure PVA membrane, the CP/PVA membranes exhibit characteristic absorption peaks at 1650 and 1685 cm^{-1}, corresponding to N–H bending and C=N stretching vibrations, respectively, and the latter of which is caused by GA cross-linking.[30,31] Therefore, the combine of CP and PVA involves physical blending and chemical cross-linking, which improved the stability of the composite membranes.[16] Fig. 3b shows the good structural stability of CP/

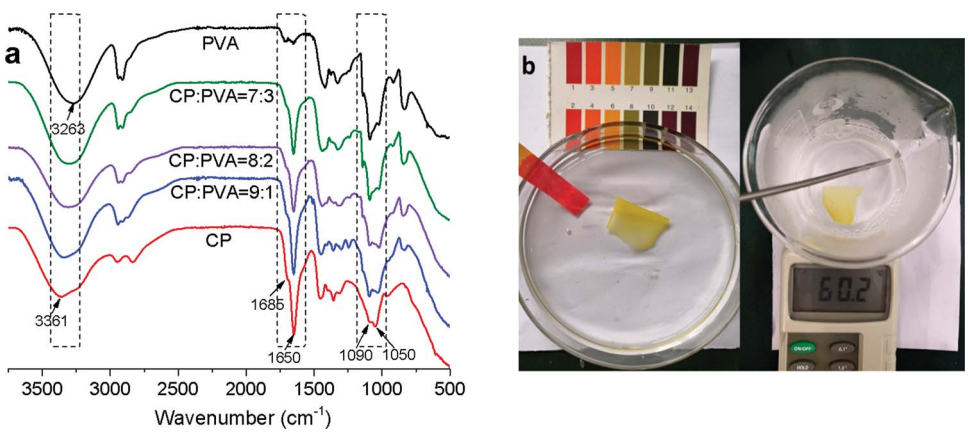

Fig. 3 Chemical structure and the stability of CP/PVA nanofiber membranes. (a) FT-IR spectra as related to CP/PVA ratio and (b) CP/PVA membranes in strong acidic solution at pH = 1 and in hot water at 60 °C.

PVA membranes, which are free from dissolution, rupture and shrinkage in HCl solution at pH = 1 or in hot water at 60 °C.

SEM images in Fig. 4 show the morphology of CP/PVA membranes with different CP/PVA ratio. PVA has an M_n being 75 000 and an alcoholysis degree being 99%. An appropriate molecular weight and drastic hydrogen bond effect provide a PVA aqueous solution with a higher viscosity and a good spinnability. Fig. 4a shows the morphology of pure PVA nanofiber membrane, which is composed of randomly interleaving nanofibers without distinct defects or conglutination. By contrast, CP is a low molecular weight polycondensate with a M_n being 10 300, and the interaction force between CP molecules is lower. As a result, the viscosity of 15 wt% CP solution is only about 20 mPa s, and the pure CP solution can only be drawn to form electrostatic atomization droplets instead of nanofibers. However, it was found that the viscosity

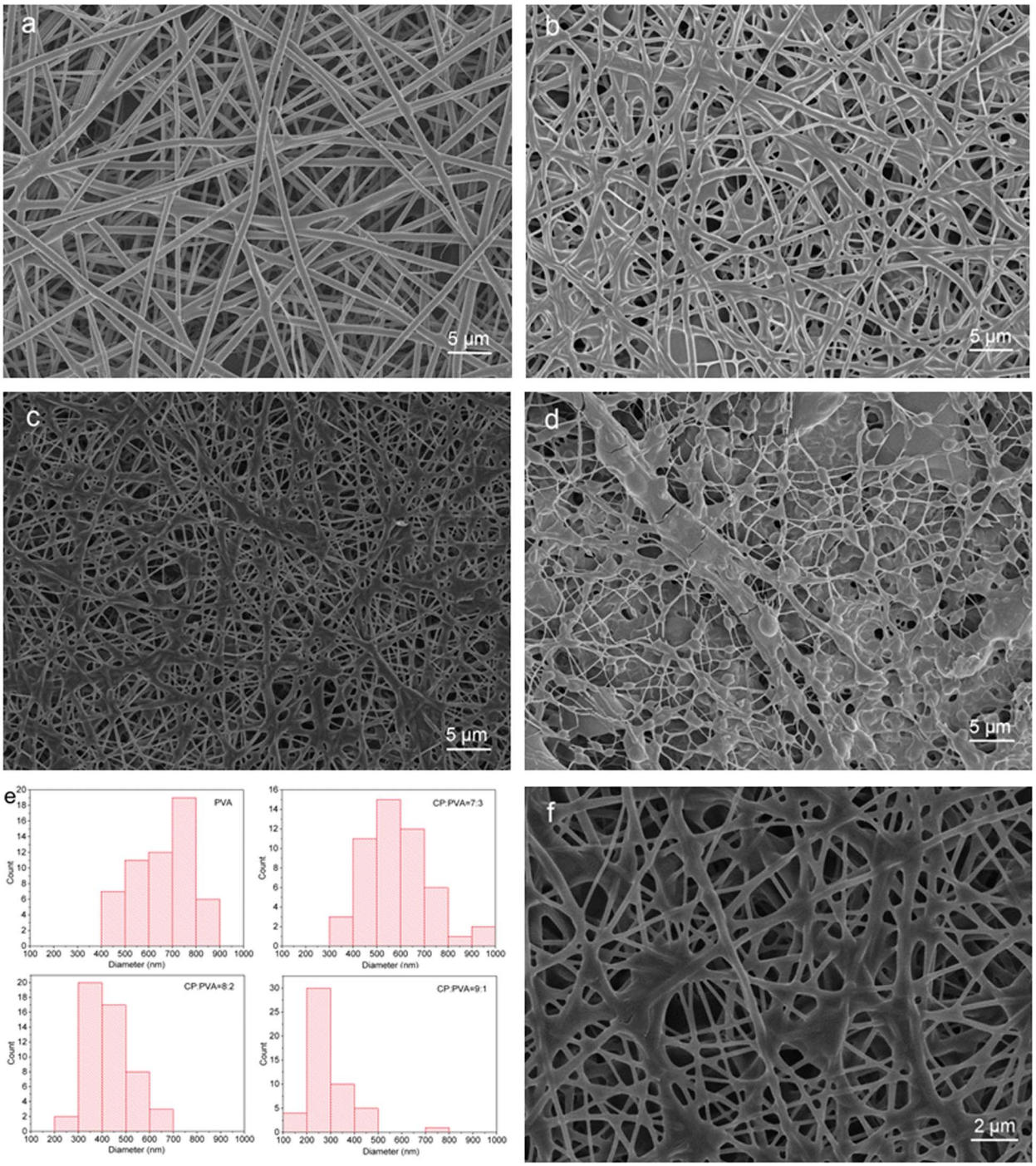

Fig. 4 SEM images of (a) pure PVA membrane, (b–d) CP/PVA nanofiber membranes with ratio of 7 : 3, 8 : 2, and 9 : 1, respectively, (e) nanofiber diameter distribution as related to CP/PVA ratio and (f) magnification of 8 : 2 sample.

of the spinning solution increased significantly with the addition of PVA. The viscosity of the CP/PVA mixed solution with mass ratio of 8 : 2 and 7 : 3 reached 315 and 525 mPa s, respectively. Fig. 4b, c and d show the SEM images of CP/PVA membranes with corresponding CP/PVA ratio of 7 : 3, 8 : 2, and 9 : 1. A constant increase in CP ratio changes the morphology of nanofibers significantly, particularly an increasing level of conglutination where nanofibers cross. In Fig. 4d, the flake-like conglutinations almost block the pores of the membranes while lots of breakage can be observed on the nanofibers. Meanwhile, the diameter of the nanofibers decreases constantly as shown in Fig. 4e. The diameter is 668.5 $\pm$ 131.7, 582.4 $\pm$ 141.1, 428.6 $\pm$ 103.9, and 284.6 $\pm$ 105.4 nm for Fig. 4a, b, c and d, respectively. Therefore, although the rise of CP proportion will increase the number of amine groups and the adsorption capacity of nanofiber membranes, it will concurrently reduce the viscosity and spinnability of the spinning solutions, thus hindering the formation of the porous structure and network morphology of the nanofiber membranes. Fig. 4f is the magnified image of the 8 : 2 CP/PVA membrane sample. In spite of the existence of a few conglutinations, the membrane retains an intact network structure and a uniform pore distribution, achieving a good balance between the nanofiber structure and the content of cationic groups. In addition, the tensile strength of 8 : 2 CP/PVA membrane is 0.87 MPa, which can meet the requirements of batch and continuous adsorption applications. In this regard, this sample was selected for further studies.

3.2 Batch adsorption study

3.2.1 Effect of pH. Since cross-linked CP/PVA nanofiber membranes was insoluble in water and PVA did not contain any cationic groups, the cationicity of CP/PVA membranes was calculated using purified CP. Colloidal titration results indicated that CP had a cationicity of 3.9, 3.5, and 1.1 mmol g^{-1} in aqueous solutions at pH 4.0, 6.4 and 9.0, respectively. Accordingly, the 8 : 2 CP/PVA membrane was calculated to have a cationicity of 3.1, 2.8, and 0.9 mmol g^{-1}. These results indicate that CP/PVA membranes carry considerable amount of cationic groups in acidic condition, and the cationicity declines significantly in alkaline environment. Fig. 1 and 3 show that there are numerous Et–NH_2, Et_2–NH and Et_3–N groups on the molecular chains of CP/PVA nanofibers. It can be found in the Bordwell pK_a table that the pK_a of Et–N^+H_3 and Et_3–N^+H is approximately 10.6 and 10.75, respectively, indicating these amine groups can be protonated even in alkaline solutions. Therefore, the presence of cationic groups is attributed to the protonation of abundant amine groups on the nanofibers.[32]

Studies revealed that Cr(VI) existed in the form of $HCr_2O_7^-$ and $Cr_2O_7^{2-}$ in acidic aqueous solutions and CrO_4^{2-} in weakly alkaline conditions.[33] Due to its high cationicity within a range of pH = 1–9, CP/PVA membranes have great affinity for Cr(VI) *via* electrostatic attraction. Fig. 5a shows that CP/PVA nanofiber membranes can efficiently adsorb Cr(VI) from simulate wastewater in a broad pH range. Furthermore, the change of the maximum adsorption capacity is consistent with the variation of the cationicity at different pH, indicating that the adsorption capacity of CP/PVA membranes is highly dependent on the number of cationic groups, *i.e.* protonated amine groups. When the solution pH decreased from 9 to 1, the equilibrium adsorption capacity (q_e) first increased and then decreased. In alkaline environment, the protonation of amine groups is constrained by excessive OH^-, which leads to the reduction of cationic groups and adversely affects the adsorption of CrO_4^{2-}. On the contrary, a large amount of H^+ combine with amine groups, which increases the number of cationic groups and makes the molecular chain expand due to the electrostatic repulsion between the same charges. As a result, CP/PVA membranes can contact and adsorb $Cr_2O_7^{2-}$ and $HCr_2O_7^-$ from wastewater readily.[34] When the solution pH declines to 1, $HCr_2O_7^-$ and $Cr_2O_7^{2-}$ gradually transform into H_2CrO_4, which weakens the electrostatic interaction and reduces the adsorption capacity, regardless of a great number of protonated amine groups.

3.2.2 Adsorption kinetics. Compared with traditional granular or spherical adsorbents, more efficient adsorbents with nanofiber networks and porous structure can be prepared conveniently and controllably by electrospinning. Fig. 5a demonstrates the rapid adsorption of Cr(VI) by CP/PVA

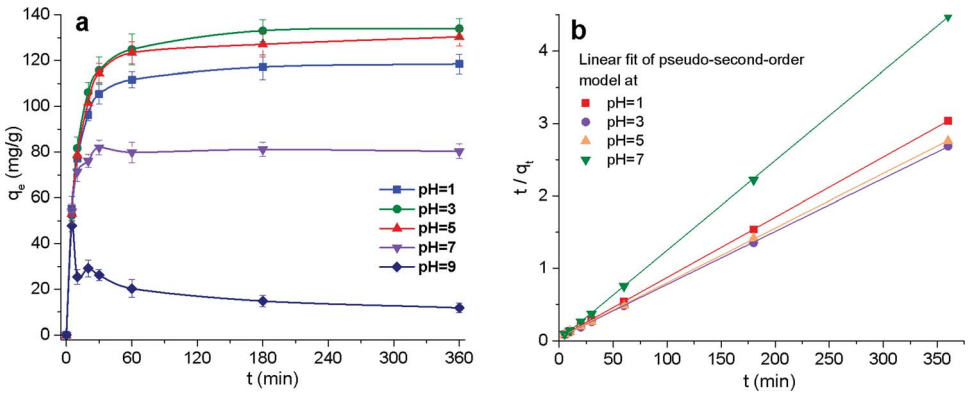

Fig. 5 The adsorption kinetics of Cr(VI) by CP/PVA membranes, (a) time profile and (b) fitting curves of pseudo-second-order model at different solution pH (experimental conditions: m = 10 mg, C_0 = 50 mg L^{-1}, V = 50 mL, T = 15 °C).

Table 1 Kinetic parameters for the Cr(VI) adsorption by CP/PVA membranes

		Pseudo-first-order model			Pseudo-second-order model		
Solution pH	$q_{e(exp)}$ (mg g^{-1})	k_1	$q_{e(cal)}$ (mg g^{-1})	R^2	k_2	$q_{e(cal)}$ (mg g^{-1})	R^2
1	118.48	9.20×10^{-3}	29.41	0.801	1.65×10^{-3}	120.24	1.000
3	133.99	8.75×10^{-3}	38.02	0.795	1.18×10^{-3}	136.61	1.000
5	130.36	8.75×10^{-3}	36.43	0.780	1.23×10^{-3}	132.45	1.000
7	80.27	5.07×10^{-3}	5.62	0.271	13.96×10^{-3}	80.71	0.999
9	11.83	4.38×10^{-3}	10.75	0.205	-5.85×10^{-3}	11.74	0.990

membranes. In acidic solution, the unit adsorption amount of Cr(VI) reaches more than 60% of the equilibrium adsorption capacity within 10 min, and further increased to 86–90% at 30 min. This high adsorption speed can be ascribed to two factors: the abundant hydrophilic groups endows CP/PVA membranes with high affinity to aqueous solutions containing Cr(VI) and the nanofiber network makes protonated amine groups contact with this anionic pollutants more easily and quickly. Notably, with a solution's pH being 9, although CP/PVA membranes can efficiently adsorb Cr(VI) in the initial adsorption stage, the adsorption capacity decreases with the time. When CP/PVA membranes are immersed in alkaline Cr(VI) solution, protonated amine groups can effectively combine $HCr_2O_7^-$ and $Cr_2O_7^{2-}$ through electrostatic interaction, thus achieving a higher adsorption amount in the initial stage. However, due to the stronger bonding force between OH^- and protonated amine group, OH^- gradually replaced the adsorbed $HCr_2O_7^-$ and $Cr_2O_7^{2-}$, resulting in the decrease of adsorption capacity in the subsequent stage. Therefore, it can be inferred that electrostatic adsorption is the dominant mechanism of Cr(VI) adsorption on CP/PVA membrane, and NaOH solution can effectively elute the adsorbed Cr(VI).

As eqn (4) and (5), pseudo-first-order model and pseudo-second-order model are employed to investigate the adsorption behaviors of CP/PVA membranes.

$$\log(q_e - q_t) = \log q_e - \frac{k_1 t}{2.303} \quad (4)$$

$$\frac{t}{q_t} = \frac{1}{k_2 q_e^2} + \frac{t}{q_e} \quad (5)$$

where q_t and q_e is separately the adsorption amount of Cr(VI) at time (t) and at equilibrium (mg g^{-1}); k_1 and k_2 is individually the rate constant of pseudo-first-order model and pseudo-second-order model.[35]

By linear regression of the experimental data, the calculated model parameters along with the correlation coefficient values are listed in Table 1, where $q_{e(exp)}$ and $q_{e(cal)}$ are the experimental and the calculated theoretical adsorption capacity, respectively. Fig. 5b shows the fitting results of pseudo-second-order model. Obviously, pseudo-second-order model fits the experimental results well for R^2 is close to 1 and the experimental data $q_{e(exp)}$ is very close to $q_{e(cal)}$. These results are consistent with the findings reported in other literatures where the adsorbents with saturated adsorption sites demonstrated similar kinetics characteristics.[36–38] In the adsorption process, protonated amine groups are the active adsorption sites of CP/PVA membranes, which are significantly dependent on the CP/PVA ratio and solution pH, and reaches saturation gradually with increasing adsorption time.

3.2.3 Adsorption isotherms. Fig. 6a shows the effect of adsorption temperature and initial Cr(VI) concentration on the equilibrium adsorption capacity of CP/PVA membranes. Table 2 and Fig. 6b show the fitting results of adsorption isotherms at different temperatures based on the Langmuir and Freundlich models. Langmuir model is shown as eqn (6).

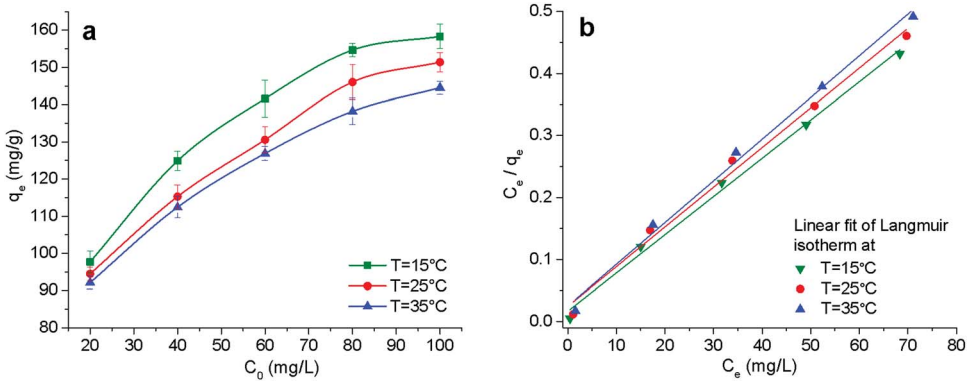

Fig. 6 The adsorption isotherms of Cr(VI) by CP/PVA membranes, (a) equilibrium isotherms and (b) fitting curves of Langmuir model for Cr(VI) adsorption of CP/PVA membrane under different temperatures (experimental conditions: m = 10 mg, V = 50 mL, pH = 3, t = 360 min).

Table 2 Isotherm parameters for the Cr(VI) adsorption by CP/PVA membranes

Temperature (°C)	Langmuir model			Freundlich model		
	q_m (mg g^{-1})	k_l	R^2	k_f	n	R^2
15	162.07	0.375	0.995	103.03	10.41	0.956
25	156.08	0.263	0.992	90.82	9.01	0.929
35	148.59	0.270	0.994	85.46	8.62	0.958

$$\frac{C_e}{q_e} = \frac{C_e}{q_m} + \frac{1}{k_l q_m} \quad (6)$$

where q_m is the maximum adsorption capacity (mg g^{-1}) and k_l is the adsorption constant. Freundlich model is shown as eqn (7).

$$\ln q_e = \ln k_f + \frac{1}{n} \ln C_e \quad (7)$$

where k_f and n are characteristic parameters of isothermal equation.[27] As can be seen from Table 2 and Fig. 6b, the adsorption experimental data presents a better fit to Langmuir model, suggesting that the adsorption behaviors match the hypothesis of the model, namely, monolayer adsorption on the uniformly distributed adsorption sites. In the case of CP/PVA membranes, the adsorption sites are the protonated amine groups, which have similar properties and distribute evenly over the surface and inside the nanofiber networks.

The electrostatic adsorption of heavy metal ions on many adsorbents also follows Langmuir isotherm model. Table 3 compares the maximum adsorption capacity of Cr(VI) by some novel adsorbents, such as GO/chitosan composites, MOFs, nanofibers and nanoparticles, under similar adsorption conditions. Comparatively, CP/PVA membrane exhibits higher adsorption capacity than most other adsorbents, which is primarily ascribed to its higher cationic group density and nanofiber network.

3.2.4 Adsorption thermodynamics. When the adsorption isotherms were investigated, the relationship between adsorption behavior and temperature was also investigated. Fig. 6a shows that the adsorption capacity of Cr(VI) decreases with increasing reaction temperature. The thermodynamics parameters are computed according to eqn (8)–(10) and listed in Table 4.

$$\Delta G = -RT \ln K \quad (8)$$

$$K = \frac{q_e}{C_e} \quad (9)$$

$$\ln K = \frac{-\Delta H}{RT} + \frac{\Delta S}{R} \quad (10)$$

It can be seen in Table 4 that $\Delta G < 0$ at three different temperatures, indicating that the Cr(VI) adsorption is a spontaneous process. $\Delta S < 0$ means the decrease randomness at the solid–liquid interface while $\Delta H < 0$ means that the adsorption involves an exothermic process. Therefore, a decrease in the reaction temperature promotes the adsorption of Cr(VI).

3.2.5 Interference of coexisting ions. Apart from Cr(VI), chromium-containing wastewater usually contains Cu^{2+}, Ni^{2+}, Zn^{2+}, and other metal ions as well. CP/PVA membranes can adsorb Cr(VI) *via* the electrostatic interaction between positively charged amine groups and negatively charged $HCr_2O_7^-$ and $Cr_2O_7^{2-}$. However, some coexisting cations and anions may compete with $HCr_2O_7^-$ and $Cr_2O_7^{2-}$ for being adsorbed concurrently. Fig. 7a shows the effects of coexisting ions on the adsorption capacity of CP/PVA membranes. In general, CP/PVA

Table 4 Thermodynamic parameters for the Cr(VI) adsorption by CP/PVA membranes

Temperature (K)	ΔG (kJ mol^{-1})	ΔH (kJ mol^{-1})	ΔS (J (mol^{-1} K^{-1}))
288 K	−3.58	−7.36	−13.24
298 K	−3.34		
308 K	−3.33		

Table 3 Maximum Cr(VI) adsorption capacity of different adsorbents

Adsorbents	Maximum adsorption capacity (mg g^{-1})	References
Porous polyacrylonitrile/graphene oxide nanofibers	382.5	39
Triethylenetetramine modified graphene oxide/chitosan composite	291.5	7
Fe_3O_4-coated cellulose acetate/chitosan nanofibers	193.2	18
CP/PVA composite nanofibers	162.1	This work
Stacked chitosan nanofibers	131.6	25
Zinc-biochar nanocomposites	102.7	40
Chitosan/PMMA composite nanofibers	92.5	41
Thiol-modified cellulose nanofibers	87.5	19
PAN/polypyrrole core/shell nanofibers	74.9	42
Silver-triazolate MOF	37.0	6
Magnetic Fe_3O_4 nanoparticles	34.9	43
Amine-functionalized MCM-41 nanoparticles	2.8	44

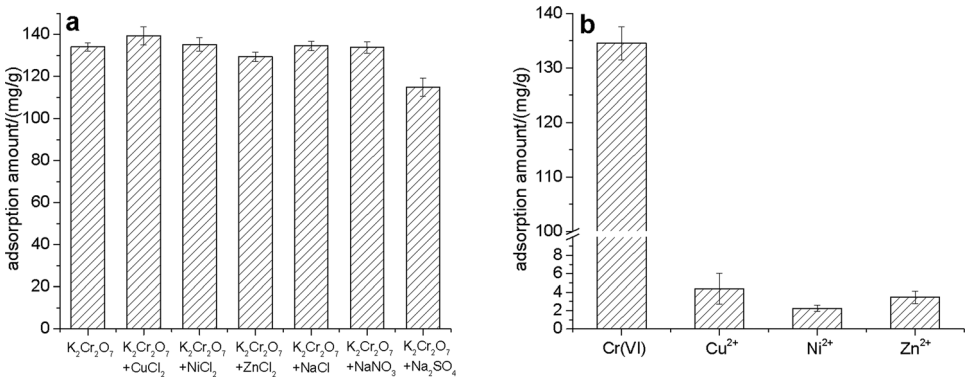

Fig. 7 Effect of coexisting ions on the adsorption of Cr(VI) by CP/PVA membranes, (a) effect of cationic and anionic ions on the adsorption capacity of CP/PVA membranes and (b) preferential adsorption of Cr(VI) among different metal ions (experimental conditions: $m = 10$ mg, $C_0 = 50$ mg L^{-1}, $V = 50$ mL, pH = 3, $T = 15$ °C, $t = 360$ min).

membranes retain satisfactory adsorption capacity in an environment with a diversity of coexisting metal ions. Although it has been reported that amine groups can adsorb Cu^{2+}, Ni^{2+}, and Zn^{2+} by chelation, the results of ICP-OES test (Fig. 7b) show that the adsorption capacities of these three metal ions are all less than 4.5 mg g^{-1}, indicating a preferential adsorption of Cr(VI). As is discussed in Section 3.2.1, the amine groups on CP/PVA membranes can be protonated even under alkaline conditions. Therefore, in acid solutions, these protonated amine groups demonstrate strong electrostatic repulsion against metal ions, which outperforms the chelation effect during the adsorption. Among the three coexisting anions, the presence of NO_3^- and Cl^- had no adverse effect on the adsorption, while SO_4^{2-} decreased the adsorption capacity by about 14%. This may be due to the interaction between SO_4^{2-} and amine groups, which decreases the number of adsorption sites.

3.2.6 Regeneration of CP/PVA membranes. It was found in the adsorption experiment that part of Cr(VI) adsorbed by CP/PVA membranes was reduced to Cr(III). Accordingly, NaOH and HCl solution were separately used to elute Cr(VI) and Cr(III) that had been adsorbed by CP/PVA membranes. Then, the adsorption capacity of regenerated CP/PVA membranes was tested. Experimental results indicated that under the same adsorption conditions, the CP/PVA membranes that were regenerated once and twice separately had adsorption capacity of 120.9 and 104.5 mg g^{-1}, which was 9.4% and 20.8% lower than that of original CP/PVA membranes, respectively. As Cr(VI) shows powerful oxidation under acidic conditions, the decrease of adsorption capacity may be due to the change of molecular structure and the decrease of cationic groups caused by redox reactions.[45,46]

3.2.7 Real wastewater treatment. To evaluate the removal ability of CP/PVA membranes for real Cr(VI) wastewater, a Cr(VI) containing wastewater sample provided by an electroplating enterprise was also treated by CP/PVA membranes. The pH of the wastewater is 4.3, the COD is 130 mg L^{-1} and the concentration of Cr(VI) is 68.2 mg L^{-1}. It was found that after 25 and 50 mg CP/PVA membranes treatment, the Cr(VI) concentration in 50 mL real wastewater decreased to 12.5 and 1.9 mg L^{-1} respectively, and the corresponding percentage removal reached 81.7% and 97.2% respectively. Meanwhile, the COD of wastewater also decreased slightly. These experimental results show that CP/PVA membranes can effectively remove Cr(VI) from real wastewater. When the dosage of the adsorbent is

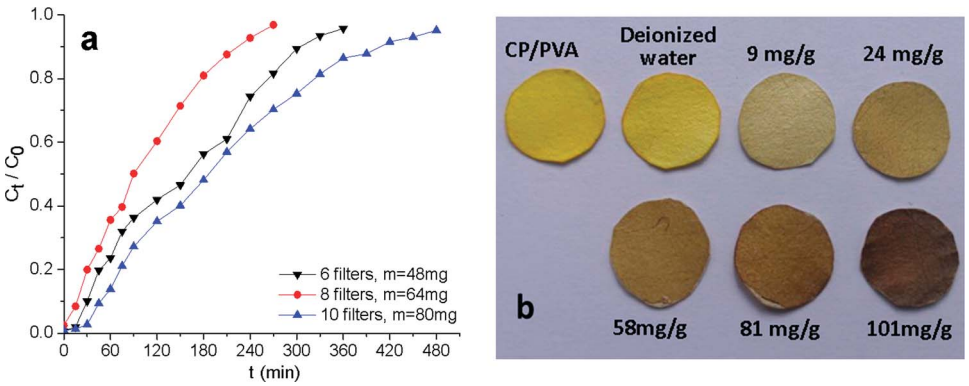

Fig. 8 Continuous adsorption and discoloration experiments, (a) breakthrough curves of filter column experiments (experimental conditions: m = 48, 64 and 80 mg, $v = 4$ mL min^{-1}, $C_0 = 10$ mg L^{-1}, pH = 3) and (b) comparison of discolored CP/PVA membranes as related to the Cr(VI) adsorption amount.

sufficient, almost complete Cr(VI) removal can be achieved. Moreover, CP/PVA membranes can also reduce the COD of real wastewater, which may be due to its adsorption of some organic pollutants in the wastewater.

3.3 Continuous adsorption and discoloration phenomenon

Continuous adsorption experiments were designed to further evaluate the potential practical application of CP/PVA membranes. In the experiments, CP/PVA membranes were trimmed into circular specimens and packed in the detachable PP filters. Several detachable filters were thereafter connected to form an adsorption column. The breakthrough curves were plotted in terms of normalized concentration C_t/C_0 *versus* time for each experiment and presented in Fig. 8a. As illustrated in Fig. 8a, although the thickness of single membrane is only about 30 μm, Cr(VI) can still be effectively removed from wastewater by a series of CP/PVA membranes. When the adsorption column is composed of 10 filters, *i.e.* the dosage of CP/PVA membranes is 80 mg, the effluent concentration of Cr(VI) remains below 0.5 mg L^{-1} after continuous treatment for more than 30 min, which is within the limit set by Chinese environmental regulation GB8978-2002 for the discharge of industrial wastewater. According to eqn (2) and (3), the amounts of adsorbed Cr(VI) per gram of dry membrane at bed exhaustion are calculated to be 88.9, 100.6 and 101.7 mg g^{-1} for 6, 8 and 10

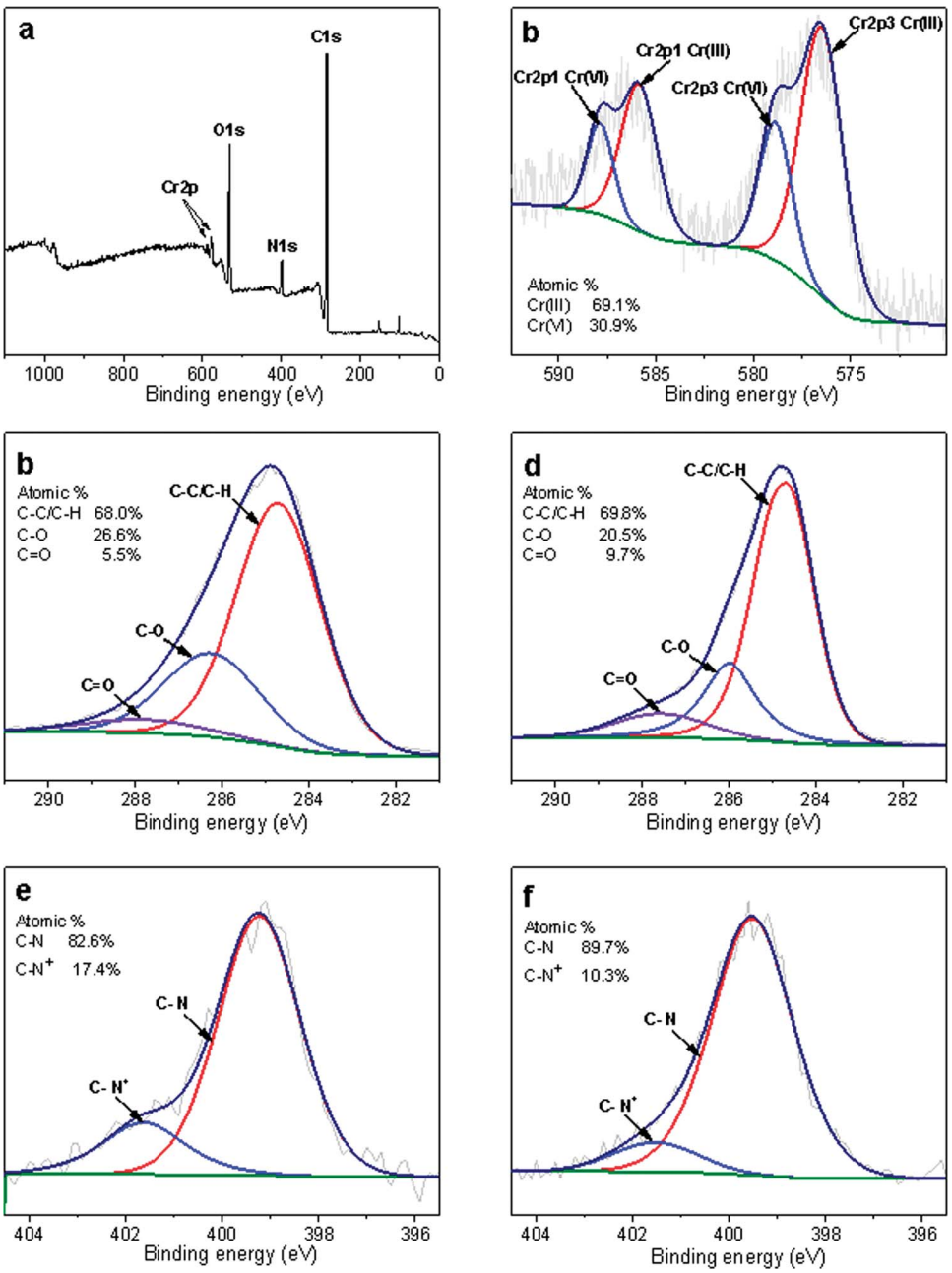

Fig. 9 XPS spectra of CP/PVA membranes, (a) survey spectrum of Cr(VI)-loaded CP/PVA membrane, (b) Cr 2p spectrum after adsorption, (c and d) C 1s spectra and (e and f) N 1s spectra before and after Cr(VI) adsorption.

filters, respectively, indicating the applicability of CP/PVA membranes in both static and continuous adsorption modes. Moreover, the adsorption efficiency can be flexibly controlled by changing the number of filters to meet different treatment requirements, and the saturated membranes can also be easily replaced.

During the experiments, it was found that CP/PVA membranes that adsorbed Cr(VI) changed the color after drying at 70 °C for 10 min. Fig. 8b demonstrates the discoloration of Cr(VI)-loaded CP/PVA membranes as related to the Cr(VI) adsorption amount. The original CP/PVA membrane and the control sample (deionized water) show the same color, whereas the experimental groups exhibit discoloration from yellowish to the dark brown corresponding to the increasing adsorption amount. The observation results indicate that the discoloration is highly correlated with Cr(VI) adsorption levels.

XPS can be used not only for the analysis of element types and valence states, but also for the semi-quantitative determination of the percentage content of different atoms.[47] To further investigate the discoloration mechanisms, Cr(VI)-loaded CP/PVA membranes were examined for XPS analysis, and the spectra were shown in Fig. 9. In the survey spectrum as Fig. 9a, CP/PVA membrane exhibit two characteristic peaks at 577.1 and 587.1 eV after adsorption, which separately corresponds to Cr $2p_{1/2}$ and Cr $2p_{3/2}$, confirming the effective adsorption of Cr(VI) by CP/PVA membrane. Fig. 9b shows the Cr 2p spectrum where the Cr element exists in the forms of Cr(III) and Cr(VI), with a ratio of about 1 : 2. It means that after being adsorbed and air-dried, Cr(VI) undergone a reduction reaction and a portion of it was reduced to Cr(III). Meanwhile, the obvious difference of C 1s spectra before and after adsorption in Fig. 9c and d also confirms the oxidation of CP/PVA membranes. In the spectra, three peaks at 284.6, 286.1 and 287.7 eV correspond to the carbon on saturated alkyl (C–C/C–H), the carbon on hydroxyl or ether bond (C–O), and the carbon on carbonyl (C=O), respectively.[48] Comparing to the blank sample, the proportion of C element in the form of C–O decreases significantly after Cr(VI) adsorption, while the proportion of C=O increases greatly. Therefore, it can be inferred that when Cr(VI) is reduced to Cr(III), some of the hydroxyl or ether bonds on CP/PVA membrane are oxidized into carbonyl or carboxyl, resulting in the increase of C=O ratio.[49] As a typical organic chromophore, the increase of C=O darkens the color of the membranes. At the same time, the reduction reaction produces dark green Cr_2O_3, which makes the color change of the membranes more obvious. These two factors may concurrently contribute to the color darkening of CP/PVA membranes, and both of them are in proportion to the adsorption amount of Cr(VI). Fig. 9e and f shows the N 1s spectra before and after adsorption. Two characteristic peaks corresponding to C–N and C–N^+ can be observed at 399.4 and 401.6 eV, respectively, and the latter is derived from the protonation of amine groups.[41] Although the binding energy of these two peaks do not change significantly after Cr(VI) adsorption, the relative content of C–N^+ decreases significantly. This confirms that the protonated amine groups of CP/PVA membranes serve as the adsorption sites in the experiments.

The commonly used Cr(VI) concentration measurement methods include ICP-MS, ICP-OES, and diphenylcarbazide spectrophotometry. However, these methods usually require sophisticated instruments and complex pretreatment. On the contrary, CP/PVA membrane provides a semi-quantitative measurement method without any complicated instrument and operation. The nanofiber structure and abundant function groups are helpful for the efficient enrichment of Cr(VI) in wastewater; the electrostatic repulsion among cations shields most of the interference caused by coexisting metal ions; and the stable chemical structure enables the membranes to be preserved and used easily. Therefore, apart from being a highly efficient adsorbent, CP/PVA membrane is also expected to be a convenient and low-cost method for semi-quantitative determination of Cr(VI) in wastewater.

4. Conclusions

In this study, a novel cationic nanofiber membrane was prepared by electrospinning a mixed aqueous solution of CP and PVA. As a cationic polycondensate, CP had high cationicity and abundant functional groups. The incorporation of PVA increased the viscosity and the spinnability of the composite electrospinning solution. With CP : PVA = 8 : 2, CP/PVA membranes achieved a good balance between the nanofiber structure and the content of cationic groups, which enabled the membranes to rapidly, massively, and selectively adsorb Cr(VI) from aqueous solutions over a wide range of pH. Equilibrium adsorption data showed good fit to Langmuir isotherm model and the maximum adsorption capacity reached 162.07 mg g^{-1} at pH = 3. The adsorption process followed pseudo-second-order model, achieving nearly 90% of the equilibrium adsorption capacity within 30 min. Besides, the adsorption of Cr(VI) was hardly affected by the coexisting metal ions. Due to the redox reaction between CP/PVA membrane and adsorbed Cr(VI), CP/PVA membrane exhibits distinct color change after Cr(VI) adsorption and the discoloration is highly dependent on the adsorption amount. Therefore, in addition to serving as a highly efficient adsorbent, CP/PVA membrane is also expected to be a convenient and low-cost method for semi-quantitative determination of Cr(VI) in wastewater.

Conflicts of interest

There are no conflicts to declare.

Acknowledgements

This work was financially supported by the Natural Science Foundation of Fujian Province of China (Grant No. 2019J01759, 2021J011021) and the Science and Technology Project of Fuzhou (Grant No. 2020-GX-4).

References

1 J. H. Li, C. L. Yao, Y. B. Liu, D. Li, B. Zhou and W. M. Cai, *J. Hazard. Mater.*, 2012, **221–222**, 56–61.

2 N. Daneshvar, D. Salari and S. Aber, *J. Hazard. Mater.*, 2002, **B94**, 49–61.
3 C. X. Zhang, Y. B. Sun, Z. Q. Yu, G. Y. Zhang and J. W. Feng, *Chemosphere*, 2018, **191**, 527–536.
4 N. Abdullah, N. Yusof, W. J. Lau, J. Jaafar and A. F. Ismail, *J. Ind. Eng. Chem.*, 2019, **76**, 17–38.
5 M. Shirzad Siboni, M. T. Samadi, J. K. Yang and S. M. Lee, *Environ. Technol.*, 2011, **32**, 1573–1579.
6 L. L. Li, X. Q. Feng, R. P. Han, S. Q. Zang and G. Yang, *J. Hazard. Mater.*, 2017, **321**, 622–628.
7 H. C. Ge and Z. W. Ma, *Carbohydr. Polym.*, 2015, **131**, 280–287.
8 A. A. Babaei, M. Ahmadi, G. Goudarzi, N. Jaafarzadeh and Z. Baboli, *Desalin. Water Treat.*, 2016, **57**, 12244–12256.
9 C. Wang, C. Xiong, Y. L. He, C. Yang, X. T. Li, J. Z. Zheng and S. X. Wang, *Chem. Eng. J.*, 2021, **415**, 128923.
10 R. Zhao, Y. Y. Tian, S. Y. Li, T. T. Ma, H. T. Lei and G. S. Zhu, *J. Mater. Chem. A*, 2019, **7**, 22559–22570.
11 H. Gao, Y. G. Liu, G. M. Zeng, W. H. Xu, T. Li and W. B. Xia, *J. Hazard. Mater.*, 2008, **150**, 446–452.
12 P. Sagitha, C. R. Reshmi, S. P. Sundaran and A. Sujith, *Eur. Polym. J.*, 2018, **105**, 227–249.
13 D. Li and Y. Xia, *Adv. Mater.*, 2004, **16**, 1151–1170.
14 X. F. Wang and B. S. Hsiao, *Curr. Opin. Chem. Eng.*, 2016, **12**, 62–81.
15 R. X. Wu, G. F. Zheng, W. W. Li, L. B. Zhong and Y. M. Zheng, *J. Nanosci. Nanotechnol.*, 2018, **18**, 5624–5635.
16 M. Aliabadi, M. Irani, J. Ismaeili, H. Piri and M. J. Parnian, *Chem. Eng. J.*, 2013, **220**, 237–243.
17 A. A. Taha, Y. N. Wu, H. T. Wang and F. T. Li, *J. Environ. Manage.*, 2012, **112**, 10–16.
18 A. Karamipour, P. K. Parsi, P. Zahedi and S. M. A. Moosavian, *Int. J. Biol. Macromol.*, 2020, **154**, 1132–1139.
19 R. Yang, K. B. Aubrecht, H. Y. Ma, R. Wang, R. B. Grubbs, B. S. Hsiao and B. Chu, *Polymer*, 2014, **55**, 1167–1176.
20 J. J. Deng, X. J. Kang, L. Q. Chen, Y. Wang, Z. Z. Gu and Z. H. Lu, *J. Hazard. Mater.*, 2011, **193**, 187–193.
21 H. Y. Ma, B. S. Hsiao and B. Chu, *Curr. Org. Chem.*, 2013, **17**, 1361–1370.
22 A. Almasian, M. Giahi, G. C. Fard, S. A. Dehdsat and L. Maleknia, *Chem. Eng. J.*, 2018, **351**, 1166–1178.
23 R. Zhao, Y. M. Li, X. Li, Y. Z. Li, B. L. Sun, S. Chao and C. Wang, *J. Colloid Interface Sci.*, 2018, **514**, 675–685.
24 R. Fang, W. X. He, H. Y. Xue and W. J. Chen, *React. Funct. Polym.*, 2016, **102**, 1–10.
25 L. Li, Y. X. Li, L. X. Cao and C. F. Yang, *Carbohydr. Polym.*, 2015, **125**, 206–213.
26 G. Z. Kyzas, N. K. Lazaridis and M. Kostoglou, *Chem. Eng. J.*, 2014, **248**, 327–336.
27 Q. Y. Yue, B. Y. Gao, Y. Wang, H. Zhang, X. Sun, S. G. Wang and R. R. Gu, *J. Hazard. Mater.*, 2008, **152**, 221–227.
28 R. B. Baird, A. D. Eaton and E. W. Rice, *Standard Methods for the Examination of Water and Wastewater*, APHA/AWWA/WEF, Washington, 23rd edn, 2017.
29 L. Jin and R. B. Bai, *Langmuir*, 2002, **18**, 9765–9770.
30 A. A. Oladipo, M. Gazi and S. Saber-Samandari, *J. Taiwan Inst. Chem. Eng.*, 2014, **45**, 653–664.
31 R. Cheng, S. Ou, M. Li, Y. Li and B. Xiang, Ethylenediamine modified starch as biosorbent for acid dyes, *J. Hazard. Mater.*, 2009, **172**, 1665–1670.
32 Y. Liu, Y. Zheng and A. Q. Wang, *J. Environ. Sci.*, 2010, **22**, 486–493.
33 M. Q. Hu, H. Y. Shen, S. Ye, Y. Wang, J. L. Zhang and S. S. Lv, *RSC Adv.*, 2018, **8**, 10686–10697.
34 L. Li, Y. X. Li and C. F. Yang, *Carbohydr. Polym.*, 2016, **140**, 299–307.
35 Y. S. Ho and G. McKay, *Water Res.*, 2000, **34**, 735–742.
36 K. Z. Elwakeel, A. A. Atia and E. Guibal, *Bioresour. Technol.*, 2014, **160**, 107–114.
37 F. K. Mahar, L. L. He, K. Wei, M. Mehdi, M. L. Zhu, J. Gu, K. Q. Zhang, Z. Khatri and I. Kim, *Chemosphere*, 2019, **225**, 360–367.
38 H. Yan, J. Dai, Z. Yang, H. Yang and R. S. Cheng, *Chem. Eng. J.*, 2011, **174**, 586–594.
39 Z. Q. Feng, X. Yuan and T. Wang, *Chem. Eng. J.*, 2020, **392**, 123730.
40 C. Gan, Y. G. Liu, X. F. Tan, S. F. Wang, G. M. Zeng, B. H. Zheng, T. T. Li, Z. J. Jiang and W. Liu, *RSC Adv.*, 2015, **5**, 35107–35115.
41 Z. Y. Li, T. T. Li, L. B. An, P. F. Fu, C. J. Gao and Z. M. Zhang, *Carbohydr. Polym.*, 2016, **137**, 119–126.
42 J. Q. Wang, K. Pan, Q. W. He and B. Cao, *J. Hazard. Mater.*, 2013, **244–245**, 121–129.
43 S. Rajput, C. U. Pittman Jr and D. Mohan, *J. Colloid Interface Sci.*, 2016, **468**, 334–346.
44 Y. X. Bao, X. M. Yan, W. Du, X. N. Xie, Z. Q. Pan, J. L. Zhou and L. S. Li, *Chem. Eng. J.*, 2015, **281**, 460–467.
45 B. Q. Ren, L. Y. Zhao, Y. L. Wang, X. X. Song, Y. Jin, F. J. Ouyang, C. W. Cui and H. W. Zhang, *RSC Adv.*, 2021, **11**, 7704–7712.
46 Y. Nakano, K. Takeshita and T. Tsutsumi, *Water Res.*, 2001, **35**, 496–500.
47 R. F. Nie, M. Miao, W. C. Du, J. J. Shi, Y. C. Liu and Z. Y. Hou, *Appl. Catal., B*, 2016, **180**, 607–613.
48 L. P. Zhu, Z. Yi, F. Liu, X. Z. Wei, B. K. Zhu and Y. Y. Xu, *Eur. Polym. J.*, 2008, **44**, 1907–1914.
49 R. Zhao, X. Li, B. L. Sun, H. Ji and C. Wang, *J. Colloid Interface Sci.*, 2017, **487**, 297–309.